Original Article

JCBFM

Journal of Cerebral Blood Flow & Metabolism
2023, Vol. 44(1) 105–117

DOI: 10.1177/0271678X231194863
journals.sagepub.com/home/jcbfm
Sage

Characterizing cerebrospinal fluid mobility using heavily T2-weighted 3D fast spin echo (FSE) imaging with improved multi-directional diffusion-sensitized driven-equilibrium (iMDDSDE) preparation

Lusen Ran[1,*], Yuqin He[1,*], Jiayu Zhu[2,3,4], Fan Long[2], Yijing Dong[2], Xiaopeng Song[2,5], Wei Wang[1] and Minghuan Wang[1]

Abstract

Cerebrospinal fluid (CSF) flow patterns and their relationship with arterial pulsation can depict the function of glymphatic system (GS). We propose an improved multi-directional diffusion-sensitized driven-equilibrium (iMDDSDE) prepared heavily T2-weighted 3D FSE (iMDDSDE-HT2) magnetic resonance imaging (MRI) method to noninvasively assess the mobility (MO) of CSF distributed in the ventricles and perivascular spaces (PVS). This method could obtain 3D high resolution (1 mm isotropic) imaging of CSF MO with full brain coverage within five min and distinguish the CSF MO across different pulse phases using a peripheral pulse unit (PPU). The MO curves had the largest amplitude value in the PVS of middle cerebral artery (11.11×10^{-9} $m^{2/s}$) and the largest amplitude growth rate in the posterior cerebral artery (189%). The average coefficient of variations (CVs) in non-pulse trigger and pulse phase 1 and 3 were 0.11, 0.10 and 0.09 respectively. The MO in older healthy participants was lower compared to the young participants, and the MO in cerebral major artery stenosis patients with acute ischemia stroke (AIS) were lower compared to those without AIS in several ventriclar ROIs ($P < 0.05$). This sequence is a clinically feasible method to effectively evaluate CSF flow patterns in human brain.

Keywords

Cerebrospinal mobility (CSF MO), glymphatic system (GS), peripheral pulse unit (PPU), perivascular spaces (PVS), magnetic resonance imaging (MRI)

Received 28 January 2023; Revised 16 June 2023; Accepted 25 July 2023

[1]Department of Neurology, Tongji Hospital, Tongji Medical College, Huazhong University of Science and Technology, Wuhan, China
[2]Central Research Institute, United Imaging Healthcare Group, Shanghai, China
[3]Paul C. Lauterbur Research Centre for Biomedical Imaging, Shenzhen Institute of Advanced Technology, Chinese Academy of Science, Shenzhen, Guangdong, China
[4]Shenzhen College of Advanced Technology, University of Chinese Academy of Sciences, Shenzhen, Guangdong, China
[5]Wuhan Zhongke Industrial Research Institute of Medical Science, Wuhan, China

*These authors contribute equally.

Corresponding authors:
Minghuan Wang, Department of Neurology, Tongji Hospital, Tongji Medical College, Huazhong University of Science and Technology, Wuhan 430030, China.
Email: mhwang@tjh.tjmu.edu.cn

Jiayu Zhu, Central Research Institute, United Imaging Healthcare Group, Shanghai 201807, China.
Email: jiayu.zhu@united-imaging.com

Introduction

The glymphatic system (GS) is a brain-wide fluid clearance pathway for removing the brain's metabolite wastes, which is reportedly impaired in various kinds of central nervous system diseases, notably Alzheimer's disease, Parkinson's disease and idiopathic intracranial hypertension.[1–3] According to the GS model, cerebrospinal fluid (CSF) flows into the brain along the periarterial space and drains out of the brain along the perivenous space. As such, CSF flow can promote the solute exchange with brain interstitial fluid (ISF) and facilitate the removal of brain metabolic wastes. The cerebrovascular beats are one of the most important driven forces for the GS.[4–6] In this case, direct evaluation of CSF mobility (MO) in perivascular space (PVS) and establishing its relationship with arterial pulsation could depict the functioning and working principle of the GS.

There are several available methods to explore CSF flow patterns by magnetic resonance imaging (MRI) in humans. For example, serial MRI after intrathecal injection of a contract agent reveals the rates of clearance of contrast material via the CSF circulation.[7–9] However, this relatively invasive procedure has not found clinical application. Through the ultra-fast magnetic resonance encephalography, Kiviniemi found that CSF flow is entrained and driven by respiratory, pulse, and very low frequency pulsation waves.[10] However, this method is highly dependent on high temporal resolution magnetic resonance technology and the algorithm for data analysis are relatively complex. The most widely used imaging method now is the diffusion tensor image (DTI), but this method can present only a surrogate for the outflow function of the GS around the medullary vein.[11–13] Recently, the team of Bito provided a method of low b-value DTI for the noninvasive imaging of CSF flow patterns[14] in the whole brain. However, this approach suffered from low spatial resolution, and drawbacks of 2D imaging, such as the dilemma to balance sensitivity and signal-to-noise ratio.

Therefore, the optimization of CSF imaging methods needs to have the following features: (1) it should be non-invasive, fast and feasible for clinical practices; (2) it should be of high resolution (especially 3D isotropic resolution), and be able to identify the key structures such as PVS; (3) it should effectively suppress signals from brain tissue and blood to minimize partial volume effects; (4) the influences of arterial pulsation should be considered. In this study, we endeavor to meet these requirements through our introduction of an improved multi-directional diffusion-sensitized driven-equilibrium (iMDDSDE) prepared heavily T2-weighted 3D fast spin echo (FSE) sequence (iMDDSDE-HT2) as an optimized method for noninvasive imaging of CSF flow patterns at 3T MR scanner.

Methods

Pulse sequence design

The iMDDSDE-HT2 sequence is composed of two main parts (Figure 1(a)). The iMDDSDE preparation part consists of a $90°_{x}$ $-180°_{-y}$ $-180°_{y}$ $-90°_{-x}$ RF pulse train and diffusion-sensitizing gradients to obtain CSF flow information in three orthogonal directions separately. In consideration of the inhomogeneity between B0 and transmit B1 field, we selected a hyperbolic secant adiabatic refocus pulse. Moreover, we designed the diffusion-sensitizing gradients to compensate for the first and second order moments ($m_0 = m_1 = m_2 = 0$), which are less sensitive to CSF flow-induced phase errors. For eddy current desensitization, we inserted two additional sets of bipolar gradients in front of this preparation module.

The second part our sequence is a 3D, high spatial resolution, heavily T2-weighted FSE acquisition, which is implemented with the Modulated flip Angle Technique in Refocused Imaging with extended echo train (MATRIX) accelerated with a compressed sensing method. As reported by Hirshler et al.,[15] cardiac cycle has great influence on CSF MO and the result we detected was mainly dependent on the pulse phase during the iMDDSDE preparation. However, the acquisition time of k-space center also affects the CSF signal that we detected. Therefore, we tried to align the starting time of iMDDSDE preparation and acquisition time of k-space center to the same pulse phase, thereby aiming to minimize signal variation caused by consecutive arterial pulsations (Figure 1(a)).

The pulse sequences were acquired on a 3 T MRI scanner (uMR 790, United Imaging Healthcare Group), using a 32-channel head coil for signal reception. The imaging parameters were as follows: scanning direction = coronal view; TE = 678 ms; slice number = 168; slice thickness = 1 mm; Field of view = $240 \times 188\,mm^2$; Matrix = 240×188; Voxel resolution: $1 \times 1 \times 1\,mm^3$; b = 0 and $100\,s/mm^2$ with three orthogonal diffusion directions. Considering inter-individual differences, TR was in the range of 3600 ms to 5400 ms; total scanning time was less than 5 min per subject. We defined the reference CSF image as the V0 image. The iMDDSDE preparation could acquire diffusion sensitized images encoded in three orthogonal directions (V1: parallel to the anterior and posterior direction, V2: parallel to the left and right direction, and V3: parallel to the inferior and superior direction; b = $100\,s/mm^2$ for all directions) (Figure 1(b)).

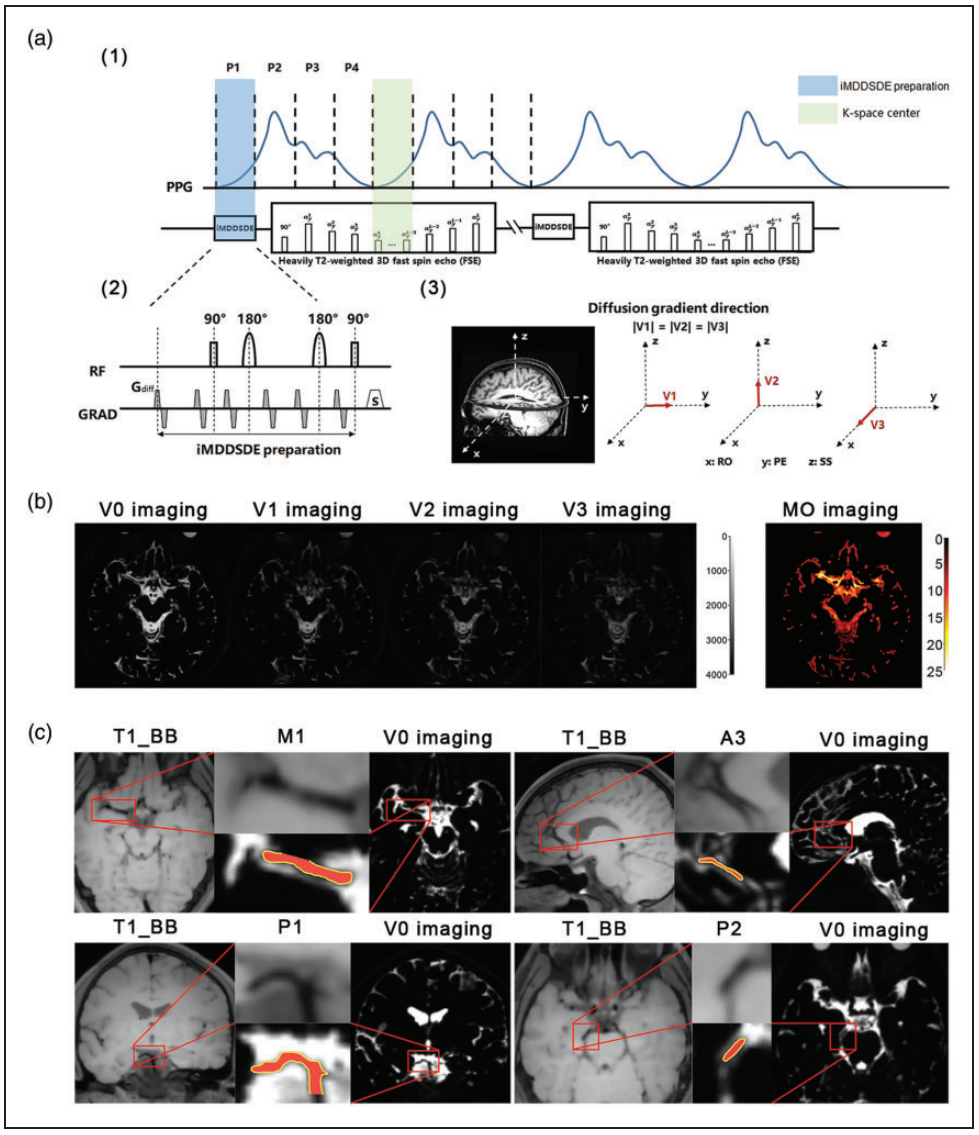

Figure 1. The pulse sequence design and imaging results of the iMDDSDE-prepared, heavily T2-weighted 3 D FSE sequence. (a) The timing diagram of this sequence. A whole pulse cycle was divided to 4 phase (phase 1, phase 2, phase 3, phase 4) averagely. (b) The V0, V1, V2, V3 and MO images of one participant. V1: parallel to the anterior and posterior direction, V2: parallel to the left and right direction, and V3: parallel to the inferior and superior direction; b = 100 s/mm^2 for all directions. Brighter color indicates greater magnitude of MO in corresponding areas in MO imaging and (c) The T1_BB and V0 images in 4 segments of cerebral arteries (M1 segment of the middle cerebral artery, A3 segment of the anterior cerebral artery, P1 segment of the posterior cerebral artery, P2 segment of the posterior cerebral artery. red) and there PVS (yellow). The arteries could be clearly discerned in our high resolution image (1 mm isotropic). The PVS was defined as the relatively high signal field around the arteries within 1 mm.

Pulse phase synchronization

The clearance rate of the GS is affected by the cardiac period.[10] By prospectively synchronizing the magnetic resonance signal acquisition with the pulse-triggered signal in peripheral vasculature, we can distinguish different flow states of CSF in different pulse phases. We defined the start of pulse systole as the beginning of pulse cycle, a whole pulse cycle was divided to 4 equal phases (phase 1, phase 2, phase 3, phase 4) averagely (Figure 1(a)). In this analysis, absence of pulse trigger represented the mean state of CSF flow across the pulse cycle. We set the trigger delay in phase 1 to zero and the trigger delay in phases 2–4 were calculated by the pulse period time of the individual participant (Take a participant with pulse period = 800 ms as an example, trigger delay in phase 1–4 were = 0, 200, 400 and 600 ms respectively).

ROI definition

PVS is the important structure of the GS,[4–6] but has hitherto eluded visualization by MRI. Aiming to access the CSF fluidity within the PVS, we can now depict the surroundings of the cerebral arteries (M1 segment of the middle cerebral artery, A3 segment of the anterior cerebral artery, P1 segment of the posterior cerebral artery, P2 segment of the posterior cerebral artery) with $1 \times 1 \times 1\,mm^3$ isotropic resolution (Figure 1(c)). We chose the PVS of the 4 arteries above as the ROI and we defined the PVS as the relatively high signal field around the arteries within 1 mm in V0 imaging. Other ventricular ROIs were also manually delineated on individual participants' V0; our selected ROIs were forth ventricle, lateral ventricle, entrance from the foramen of Monro, Sylvian fissure, prepontine cistern, and anterior horn of the lateral ventricle, as represented in supplemental Figure 1. We also chose the ROI around the superior sagittal sinus (SSS) to represent the area around the venous sinus. Due to a previous finding that the anterior horn of the lateral ventricle has a low MO as expected for "free-water" with low MO,[14] we selected this region as a reference for the other ROIs.

Imaging analysis

First, the data acquired from different directions (V0-V3) was motion-corrected with rigid registration using mcflirt of FSL. Then, the CSF mobility (MO) was calculated as follows:

$$MO = [Ln(S_{V1}/S_{V0}) + Ln(S_{V2}/S_{V0}) + Ln\ (S_{V3}/S_{V0})/3(b0\text{–}b1)]$$

Where S_{vn} (n = 0,1,2,3) is the intensity of data Vn; b1 is the b-value of V1-V3 and b0 is the b-value of V0. The fluidity of CSF is represented by MO, where a greater MO value indicates stronger fluidity. In the imaging results (Figure 1(b)) intensity of red color represents the magnitude of MO.

As show in a previous study,[14] the limit of the apparent diffusion coefficient (ADC) as b decreases to zero can be used to estimate the variance of the velocity distribution of a pseudorandom flow. Furthermore, we define MO as the ADC acquired at a relatively low b-value ($b = 100\,s/mm^2$), which describes the covariance of velocity distribution induced by flow and molecular diffusion and indicates the intensity of local stirring.

In-vivo experiment design

This study was authorized by Medical Ethics Committee of Tongji Hospital, Tongji Medical College Huazhong University of Science and Technology (TJ-IRB20220455). All experiments were performed in accordance with the Declaration of Helsinki and Good Clinical Practice.

We recruited four groups of participants at the Physical Examination Center and Neurology Department of Tongji Hospital from March 2022 to June 2023: young healthy group (healthy participants aged 18–30 years old), older healthy group (healthy participants over 45 years old), cerebrovascular stenosis (CS) group (patients diagnosed with major intracranial artery stenosis but without acute ischemic stroke (AIS)) and CS-AIS group (patients diagnosed with CS and AIS onset within one week). Informed and signed consent was obtained from all participants. Our inclusion criteria for were as follows: (1) Over 18-years old; (2) could participate in an MRI exam; (3) not diagnosed with organic disease of the nervous system (healthy group); (4) able to voluntarily sign the informed consent form. Our exclusion criteria were as follows: (1) claustrophobia or other serious mental disorders; (2) metallic implants such as nail plates, insulin pumps, vascular stents, or dentures; (3) evidence of organic disease of the nervous system upon examination (healthy group); (4) evidence of AIS upon examination (CS group).

The diagnoses of AIS and CS were made from a previously-acquired general structural MRI and computered tomograhy angiography (CTA) scan. Healthy participants were also given a general structural MRI and magnetic resonance angiography (MRA) scan of the head to further exclude the possibility of any neurological diseases. Two experienced radiologists assessed the image to exclude organic disease of the nervous system, including stroke, tumor, intracranial infection, brain trauma, neurodegenerative disease, demyelinating disease, etc.

Before the start of the scan, pulse rate of the participants was detected. Next, the young healthy participants were scanned with the iMDDSDE-HT2 sequence (V0-V3) for pulse phase 1–4 to find the pattern of altered MO across a complete pulse cycle. Then we compared the clinical application prospect of iMDDSDE-HT2 sequence for pulse phase 1, phase 3 and no pulse trigger. The young healthy participants were scanned this sequence three time to test the signal stability across different pulse phases. The older healthy participants were scanned to test the influence of age on CSF MO. CS and AIS patients were scanned to compare the CSF MO within these two groups.

Statistical analysis

GraphPad Prism 8.0 software and IBM SPSS Statistics 20.0 were used for Statistical analysis. All data sets

were tested for normal distribution using Kolmogorov-Smirnov test. Independent sample t-test was used to analyze the differences of MO in ROIs relative to that in the reference region, i.e. anterior horn of the lateral ventricle. Independent sample t-test was also used to analyze the differences of MO by region among the two participant groups. Paired samples t-test was used to analyze the differences of MO across different pulse phases. $p < 0.05$ (two-sided) represented a statistically significant difference. All statistical charts were produced by GraphPad Prism 8.0 software.

Results

Optimization and evaluation

We recruited 81 participants for the test of iMDDSDE-HT2 sequence. After excluded 2 participants with organic diseases of the nervous system, 7 young, 7 older healthy participants, 10 CI patients and 10 CS-AIS patients were finally involved (see supplemental Table 1). Before the optimization of iMDDSDE preparation, we had involved 45 participants for testing of various versions of the iMDDSDE-HT2 sequence.

Supplemental Figure 2 (a, b) shows the benefits of utilizing first and second order moment-compensated diffusion-sensitizing gradients. As for V3 imaging, zeroth moment-compensated gradients usually resulted in CSF flow-induced signal loss in the parietal area and phase mismatch errors surrounding the lateral ventricle. A phantom filled with water was scanned at the room temperature of 18°C after setting still for 30 min; phantom V0 and MO imaging results were shown in supplemental Figure 2 (c) in the Data Supplement. The mean MO of the whole phantom was 1.92×10^{-9} m^2/s, which fell within the expected range of MO values.[16]

The CSF MO changes with pulse cycle

Figure 2 displays that pattern of MO changes in young healthy participants across the entire pulse cycle, as divided into temporal quartiles. The MO change curves showed the tendency to increase and then decrease for of all ROIs, with the peak value occurring at phase 3 of a pulse period. The ROI for PVS of M1 had the largest amplitude (11.11×10^{-9} m^2/s) and The ROI for PVS of P1 had largest increase (189%) between pulse phase 1 to phase 3, while the ROI for the anterior horn of the lateral ventricle had the lowest amplitude and increasing percentage (1.45×10^{-9} m^2/s, 34%).

Stability evaluation

The results above showed MO in pulse phase 1 and 3 could be the valley and peak values of MO in a pulse cycle. Then we compared the clinical application prospect of this sequence for pulse phase 1, phase 3 and no pulse trigger. We calculated the mean, standard deviation (SD) and CV (SD/mean) by regions for the triplicate scans in healthy young participants; smaller CV indicates more stable results. Mean CVs of each ROI in different phases were 0.11 in non-pulse triggered phase 0.10 in phase 1 and 0.09 in phase 3 respectively (Table 1). We next contrasted MO values in the ROIs to reference values in the anterior horn of the lateral ventricle. For no pulse trigger, MO values at the entrance from the foramen of Monro, the prepontine cistern, PVS of M1, A3 and P2 were larger than in the reference region (9.47 vs 5.12, $p < 0.001$; 9.29 vs 5.12, $p = 0.010$; 11.15 vs 5.12, $p = 0.006$; 7.24 vs 5.12, $p = 0.037$ and 8.95 vs 5.12, $p = 0.025$ respectively). For pulse phase 1, MO at the entrance of the foramen of Monro and PVS of M1 exceeded that in the reference region (6.14 vs 4.56, $p = 0.003$ and 7.43 vs 4.56, $p = 0.047$ respectively). For pulse phase 3, MO at the entrance of the foramen of Monro, the Sylvian fissure, the prepontine cistern, PVS of M1, A3 P1 and P2 were larger than in the reference region (12.21 vs 7.62, $p < 0.001$; 9.94 vs 7.62, $p = 0.034$; 14.98 vs 7.62, $p = 0.002$; 17.78 vs 7.62, $p = 0.002$; 11.07 vs 7.62, $p = 0.021$; 13.55 vs 7.62, $p = 0.014$ and 13.80 vs 7.62, $p = 0.011$ respectively). For no pulse trigger, pulse phase 1 and 3, MO around the SSS was significantly lower than in the reference region (4.17 vs 5.12, $p = 0.012$; 3.78 vs 4.56, $p = 0.019$; 5.94 vs 7.62, $p = 0.007$ respectively).

Comparation of different pulse phases

Figure 3(a) to (c) shows the MO imaging results for no pulse trigger, pulse phase 1, and pulse phase 3 of one representative young participant. Globally, the images of pulse phase 1 were darkest and images of pulse phase 3 were lightest. This result shows that the CSF MO of the whole brain was higher during pulse phase 3 than in pulse phase 1, which was confirmed by statistical analysis of different ROI results (Figure 3(d)). MO in all ROIs were significantly lower at pulse phase 3 than at pulse phase 1 (anterior horn of the lateral ventricle: 4.56 vs 7.62, $p = 0.019$; forth ventricle: 4.17 vs 8.06, $p = 0.009$; lateral ventricle: 4.25 vs 7.33, $p = 0.005$; entrance from the foramen of Monro: 6.14 vs 12.21, $p = 0.002$; sylvian fissure: 4.31 vs 9.94, $p = 0.002$; prepontine cistern: 6.04 vs 14.98, $p = 0.002$; PVS of M1: 7.42 vs 17.78, $p = 0.007$; PVS of A3: 4.88 vs 11.07, $p = 0.003$; PVS of P1: 5.68 vs 13.55, $p = 0.002$, PVS of P2: 6.19 vs 13.80, $p = 0.009$ and around SSS 5.94 vs 3.78, $p = 0.011$). Corresponding MO values for no pulse trigger fell between pulse phase 1 and phase 3 values.

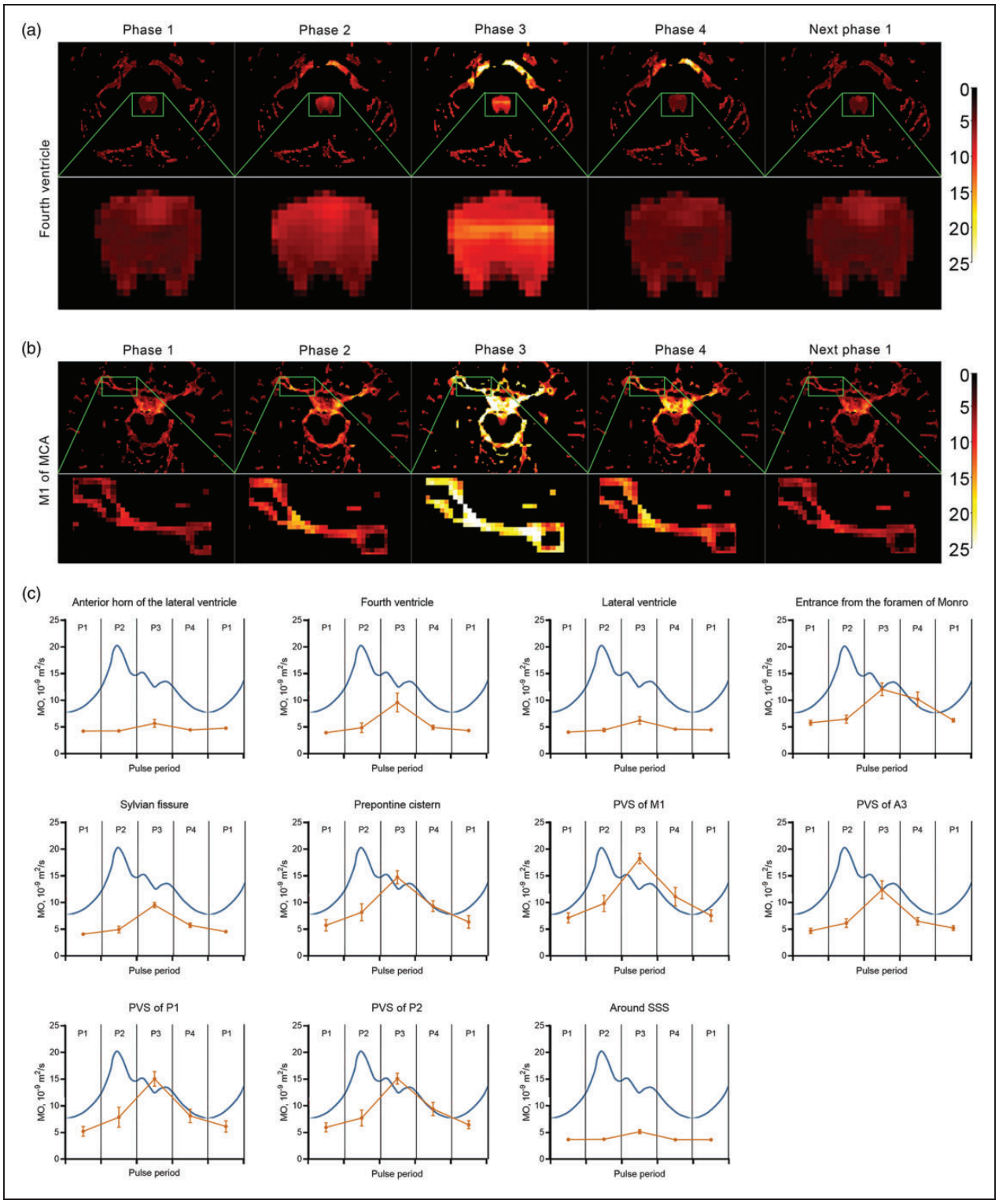

Figure 2. The change patterns of MO in a whole pulse period in healthy young participants. (a, b) The MO changes in the fourth ventricle (a) and middle cerebral artery M1 segment (b) of one young participant. MO images were brightest at phase 3 and (c) MO change curves (yellow) in ROIs (anterior horn of the lateral ventricle, fourth ventricle, lateral ventricle, entrance of the foramen of Monro, sylvian fissure, prepontine cistern, M1 segment of the middle cerebral artery, A3 segment of the anterior cerebral artery, P1 segment of the posterior cerebral artery, P2 segment of the posterior cerebral artery and area around superior sagittal sinus) in pulse cycle (blue). The MO change curves showed the tendency to towards a zenith during phase 3 of the pulse period and then decline.

Table 1. Statistical results of MO obtained of no pulse trigger, pulse phase 1 and pulse phase 3 in young healthy participants.

ROIs	Anterior horn of the lateral ventricle	Fourth ventricle	Lateral ventricle	Entrance from the foramen of Monro	Sylvian fissure	Prepontine cistern	PVS of M1	PVS of A3	PVS of P1	PVS of P2	Around SSS
No pulse trigger											
Mean, 10^{-9} m^2/s	5.12	5.68	4.91	9.47	6.06	9.29	11.15	7.24	8.66	8.95	4.17
SD, 10^{-9} m^2/s	0.56	0.56	0.42	0.97	0.84	1.02	1.02	0.88	1.11	1.08	0.38
CV	0.10	0.10	0.08	0.10	0.14	0.12	0.10	0.13	0.15	0.11	0.09
p trend*	NA	0.359	0.564	<0.001	0.089	0.010	0.006	0.037	0.055	0.025	0.012
Pulse phase 1											
Mean, 10^{-9} m^2/s	4.56	4.18	4.25	6.14	4.31	6.04	7.43	4.88	5.68	6.19	3.78
SD, 10^{-9} m^2/s	0.44	0.32	0.34	0.69	0.41	0.79	0.59	0.54	0.70	0.64	0.46
CV	0.09	0.08	0.08	0.11	0.10	0.12	0.08	0.11	0.12	0.11	0.12
p trend*	NA	0.279	0.237	0.003	0.483	0.195	0.047	0.562	0.282	0.094	0.019
Pulse phase 3											
Mean, 10^{-9} m^2/s	7.62	8.05	7.34	12.21	9.94	14.98	17.78	11.07	13.55	13.80	5.94
SD, 10^{-9} m^2/s	1.13	0.58	0.65	0.84	0.70	0.90	1.11	1.05	1.09	0.89	0.82
CV	0.13	0.09	0.08	0.08	0.07	0.07	0.07	0.10	0.09	0.07	0.12
p trend*	NA	0.614	0.277	<0.001	0.034	0.002	0.002	0.021	0.014	0.011	0.007

A3: A3 segment of the anterior cerebral artery; CV: coefficient of variation; NA: not available; MO: mobility; M1: M1 segment of the middle cerebral artery; PVS: Perivascular space; P1: P1 segment of the posterior cerebral artery; P2: P2 segment of the posterior cerebral artery; SD: standard deviation; SSS: Superior sagittal sinus.

*p value at each ROI was calculated by the paired samples t-test compared against the ROI of the anterior horn of lateral ventricle.

The CSF MO decreased in older healthy participants

We compared the MO results of seven young and seven older participants (Figure 4). The pulse phase 3 results in 1 older participant was excluded because of poor imaging result. For no pulse trigger, MO at the entrance of the foramen of Monro was higher in young participants than in the older group (9.47 vs 6.50, $p = 0.027$). For pulse phase 1, MO in the fourth ventricle, lateral ventricle, Sylvian fissure, and anterior horn of the lateral ventricle was higher for young participants compared to the older group (4.19 vs 2.89, $p = 0.006$; 4.25 vs 2.39, $p = 0.006$; 4.34 vs 3.51, $p = 0.045$ and 4.57 vs 3.68, $p = 0.022$ respectively). For pulse phase 3, MO in the lateral ventricle, entrance from the foramen of Monro, sylvian fissure, anterior horn of the lateral ventricle and around the SSS was higher for young participants compared to the older group (7.34 vs 4.61, $p = 0.013$; 12.21 vs 8.24, $p = 0.046$; 9.94 vs 6.57, $p = 0.032$; 7.62 vs 4.26, $p = 0.006$ and 5.94 vs 3.74, $p = 0.004$ respectively).

The CSF MO decreased in AIS patients

We compared the MO results of 10 CS and 10 CS-AIS patients (Figure 5). For no pulse trigger, MO in lateral ventricle, prepontine cistern, PVS of M1, P1 and P2 was lower for the CS-AIS group compared to the CS group (3.48 vs 4.62, $p = 0.047$; 7.96 vs 11.09, $p = 0.017$; 7.52 vs 10.54, $p = 0.040$; 5.84 vs 8.42, $p = 0.039$ and 5.59 vs 9.04, $p = 0.034$ respectively). For pulse phase 3, the MO prepontine cistern and PVS of P2 were lower for the CS-AIS group compared to the CS group (10.74 vs 13.84, $p = 0.008$ and 8.09 vs 12.29, $p = 0.013$ respectively).

Discussion

We present a novel iMDDSDE-HT2 sequence to assess CSF MO for functional imaging of the GS in healthy adults and in groups of cerebrovascular stenosis patients. The primary advantage of our imaging method is presented by the high spatial resolution with a 1 mm scale for the case of the cerebral artery and heavily T2-weighted contrast, which is a key requirement for accurate evaluation of ROIs such as PVS. A second advantage of our method lies in the implementation of a PPU to explore the relationship between CSF mobility and pulse cycle. Previous work indicates that CSF flow has a quick response to heart beats,[17] so we design a prospective gating strategy to acquire the CSF signal from different pulse phases. The third advantage lies in its simplicity and noninvasive nature, the sequence can map CSF MO within only five min on 3 T scanner, which should favor the clinical promotion of this approach.

Our iMDDSDE-HT2 sequence integrates some features of existing research methods, and entails an optimization in spatial resolution and workflow. Compared with traditional diffusion approaches with echo planar image (EPI) readout, our method enables

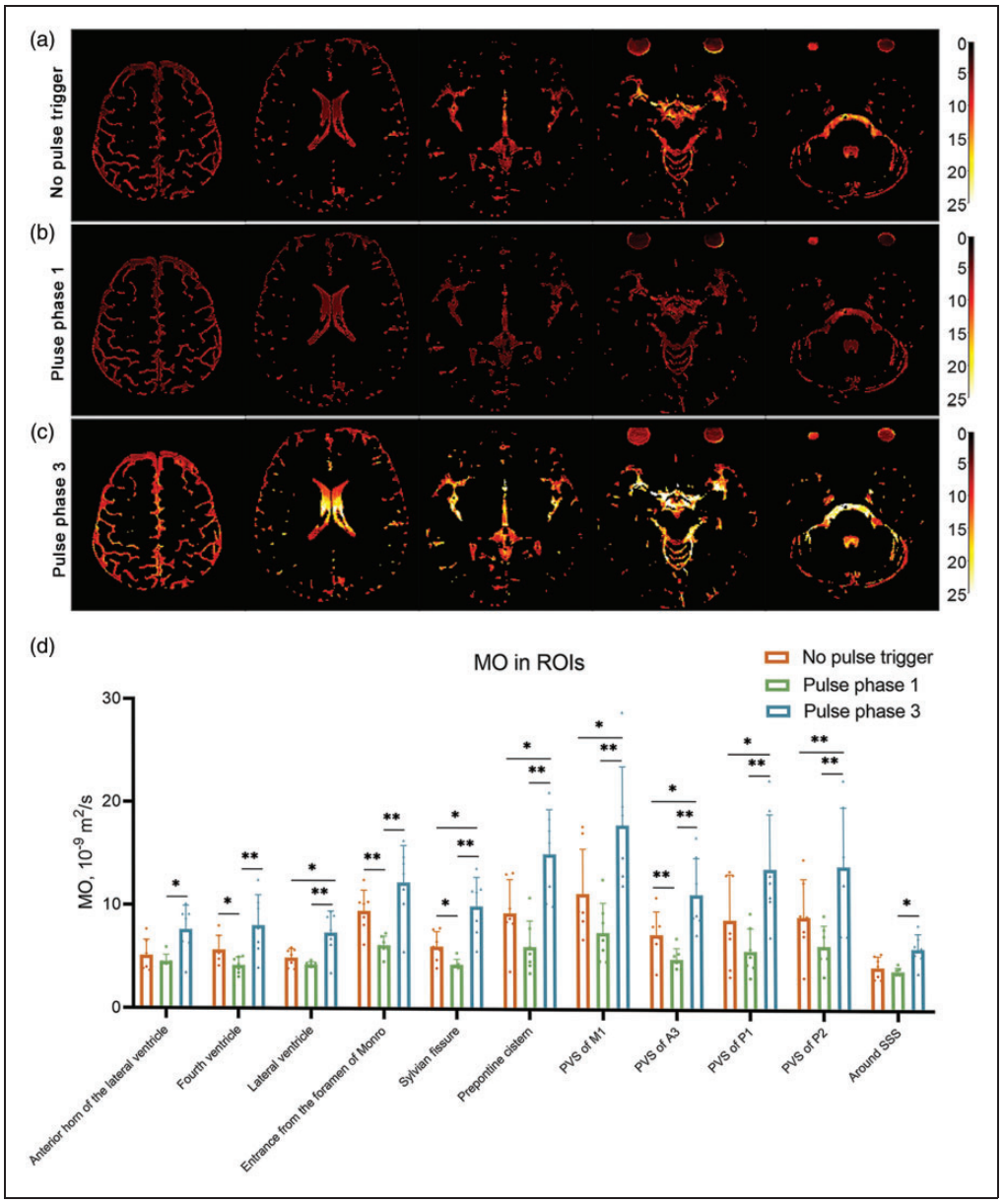

Figure 3. The results for different pulse cycles in young healthy participants. (a–c) The MO images of no pulse trigger (a), phase 1 (b) and phase 3 (c) for a representative healthy young participant. The images of pulse phase 3 are brighter than for pulse phase 1, indicating globally higher MO. (d) The statistical results in different ROIs across the phases of systole/diastole. The MO was higher in all ROIs at pulse phase 3 compared to pulse phase 1, with intermediate MO for no pulse trigger.

the use of a long echo time FSE readout, which enables significant improvements in image resolution, quality, and distortion. As the diffusion-sensitized magnetization is stored in the longitudinal direction after iMDDSDE preparation, our approach further facilitates the use of 3D readout sequences. As for the optimization of b-value, we propose that $b = 100$ is an optimal choice for low b-value acquisition, considering the relatively longer fast spin echo train for heavily T2-weighted imaging.[14] While higher spatial resolution necessarily calls for acquisition of larger k-space data, we need to combine acquisition lines from multiple excitation shots into one k-space. In this situation, the phases evolved by physiological flow of CSF between different excitations are apt to be a major source of artefacts emerging during image reconstruction. We therefore tried to minimize the phase difference by utilizing the second order moment nulling gradient design, which improved the reproducibility of repeated tests. As such, our sequence performed well in repetition at this high resolution and sensitivity. Giving average CVs around 0.1, irrespective of pulse

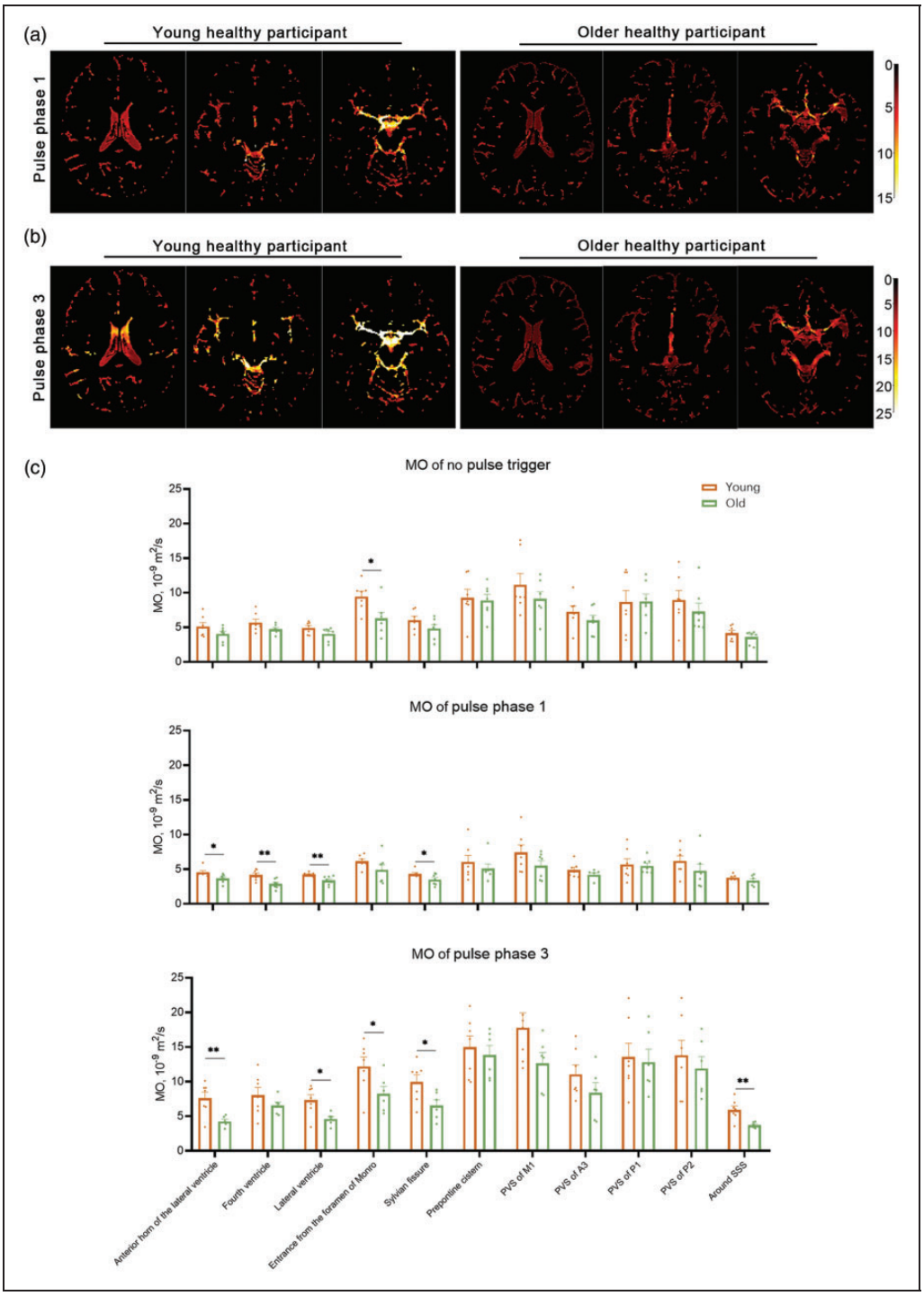

Figure 4. The comparation of the MO results in healthy young and older participant groups. (a, b) MO imaging results of young and older participants. The MO imaging of phase 1 (a) and phase 3 (b) were both brighter in the younger healthy participant. (c) The statistical plot of mean MO results in young and older healthy participant groups. MO for no pulse trigger in the entrance of the foramen of Monro was higher in the young group. MO for phase 1 in the fourth ventricle, lateral ventricle, sylvian fissure, and anterior horn of the lateral ventricles were higher for young participants compared to the older group. MO for phase 3 in the lateral ventricle, entrance from the foramen of Monro, sylvian fissure, anterior horn of the lateral ventricle and area around superior sagittal sinus (SSS) was higher for young participants compared to the older group.

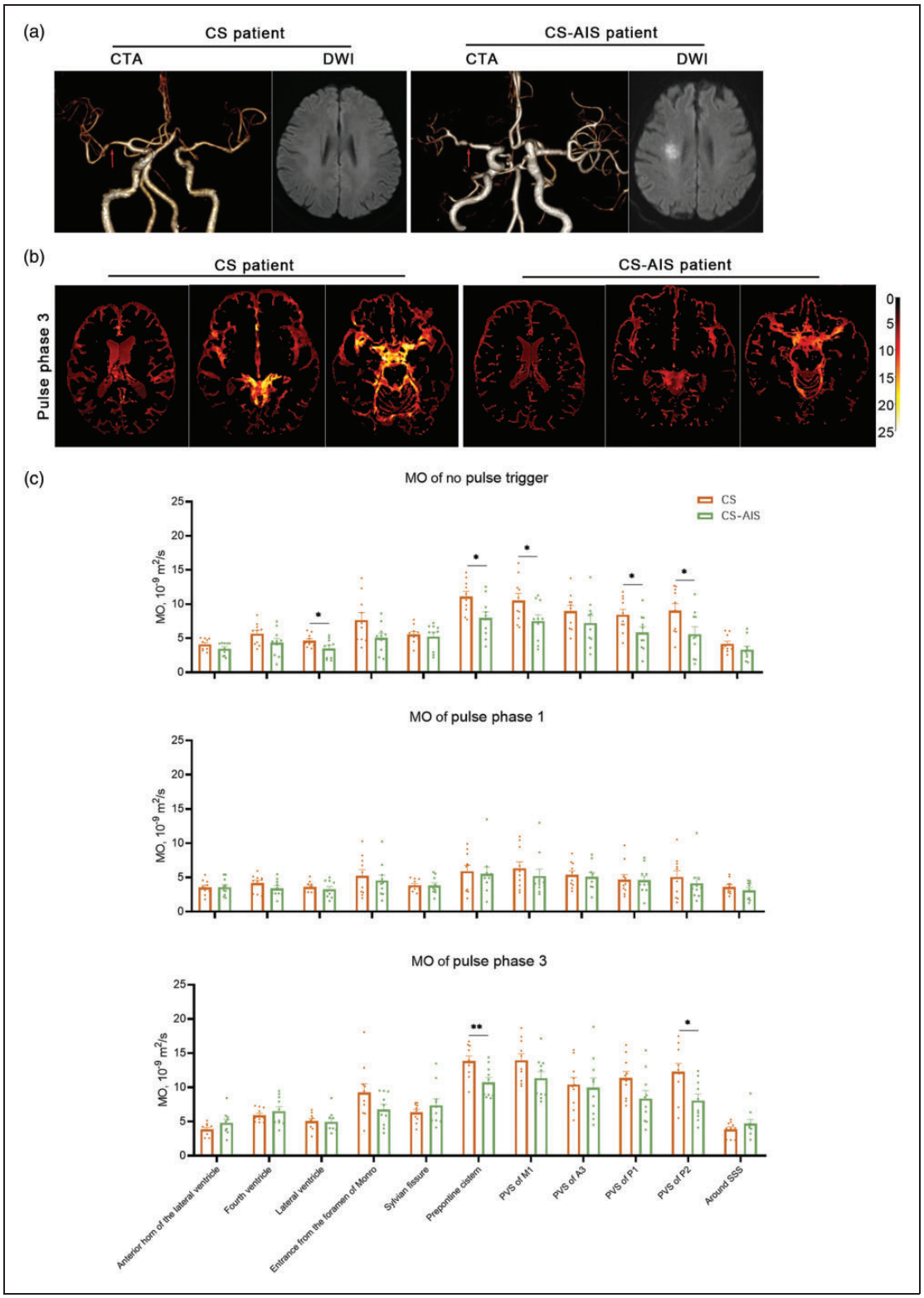

Figure 5. The comparation of the MO results in cerebrovascular stenosis (CS) and acute cerebral infarction (CS-AIS) patient groups. (a) CTA and DWI results of CS and CS-AIS patients. Both representative patients showed left middle cerebral artery stenosis (red arrow), and the CS-AIS patient had high signal intensity on DWI in the right corona radiata region. (b) MO imaging results of CS and CS-AIS participants. The MO imaging of phase 3 was brighter in the CS patient and (c) The statistical plot of mean MO results in CS and AIS groups. MO for no pulse trigger was lower in the lateral ventricles, prepontine cistern, PVS of M1, P1 and P2 of the for CS-AIS group compared to the CS group. MO for pulse phase 3 was lower in the prepontine cistern and PVS of P2 for the CS-AIS group compared to the CS group.

phase, which should enable the sensitive detection of perturbations. Because the CSF MO is averaged across the scanning time, a CV around 0.1 is a satisfactory representation of a constantly changing physiological signal.

The improved sensitivity of our method allowed us to identify the anterior horn of the lateral ventricle as an ROI with low CSF fluidity, albeit not constituting "free-water" as the previous reported.[14] Considering that brain temperature is about 37°C, the MO value (5.12 for no pulse trigger) in the anterior horn of the lateral ventricle exceeds the expected for of "free-water" at this temperature ($2.90–3.22 \times 10^{-9}$ m^2/s).[16] We also found significantly higher MO in the reference region for pulse phase 3 compared to pulse phase 1 (Figure 2(d)), and the MO around SSS was lower than the reference region (Table 1), which again indicates violation of what would be expected for a "free-water" signal.

Our results showed plots of MO changes across the cycle showed the tendency to increase and then decrease in different ROIs. The peak of MO signal followed by the peak of pulse systole peak in all ROIs (Figure 2). CSF in the PVS of cerebra arteries will be directly affected by the cerebral vascular pulsation, which likely accounts for these ROIs showing the largest percentage increase among the ROIs examined. As the anterior horn of the lateral ventricles ROI does not lie close to any major vessels, it showed the lowest percentage increase (34%). Therefore, present results support the conclusion that pulse pulsation is one of the main driving forces of CSF flow, and that fluidity of the CSF changes periodically in phase with each pulsation cycle. Previous study on rodents also found the regular on CSF fluidity and artery/cardiac contraction.[18,19] We concluded that during the systole, the mechanical force of the artery encourage the flow of CSF, and the CSF flow peak had a short delay from the artery systole peak. Further, in most ROIs, MO of pulse phase 1 and 3 were smaller than these for no pulse trigger (Table 1), which means considering the artery pulsation could increase the stability. Meanwhile, CSF MO in phase 3 was the largest when compared to others (Figure 3). The peak time of CSF MO may better reflect differences within and between individuals with well stability. Thus, we recommend this iMDDSDE-HT2 sequence of pulse phase 3 for clinical applications in the GS evaluation.

To further examine the basis of population differences in CSF MO, we compared the results in groups of healthy young and older participants, with the clear finding that MO declined in most ventriclar ROIs with healthy aging and that MO in PVS ROIs was likewise lower in the older group. We suppose that declining MO is related to age-related physiological function changes, such as cardiac output or vessel elasticity, or the development of atherosclerosis. Since vascular pulsation is the main driving force of CSF flow, any decrease in vascular elasticity caused by atherosclerosis would likely impair CSF flow. Testing this prediction should be the subject of future investigations of clear clinical relevance.

To further examine potential clinical applications of the sequence, we compared the results in groups of CS and CS-AIS patients, with the finding that MO lower in CS-AIS patients in several ROIs. This results seems consistent with previous reports that the glymphatic circulation is disrupted during the acute phase of cerebral infarction.[20,21] We plan further studies aiming to test our prediction that a further optimization of our sequence has the potential to predict AIS in patients with CS.

CSF flows in from the periarterial space, undergoes mixing with brain ISF, and then exits from the perivenous space, carrying with it metabolic waste.[4–6] As such, PVS is distinctly the most important pathway of the GS. The most widely used functional imaging method for GS is currently the DTI-ALPS, which can only capture an approximation of the outflow function of the GS around the medullary vein.[11–13] In contrast, the advantage of our sequence is that we can evaluate CSF flow across the whole brain. The team of Wen has also tested the paravascular CSF fluid dynamics by using the dynamic diffusion-weighted imaging (dDWI) and coupling the pulse signal.[22] In order to identify the ROIs of PVS, they proposed a calculation model to define dynamic characters of CSF, which requires relative high computation complexity. As the imaging method is based on 2D EPI readout with high temporal resolution, it may still be restricted to partial volume effects when extracting CSF signal from ROIs of PVS.

We note some limitations of our MR sequence. First, the CV of our results were somewhat higher when compared with the method of Yoshitaka.[14] We suppose this may be a trivial consequence of our higher sensitivity and spatial resolution, which might be ameliorated by use of appropriate trade-offs in resolution. Second, in the interest of brief scanning time, we only acquired three spatial directions. We suppose that increasing the number of spatial directions could yield a more sensitive evaluation of CSF mobility. Third, although we expected the CSF MO changes with the pulse cycle, our time resolution is still too low to evaluate the detailed time-dependent characteristics of CSF movement. Furthermore, our approach does not yet accommodate effects of respiration and vasomotor waves on the movement of CSF. A more generalized approach will call for further optimization of our methods. Finally, there may be some delay

between the pulse signal we monitor and the actual cerebral vascular pulsation due to hand symphathetic nervous system effects on smooth muscle tone. However, this is already a feasible method to monitor blood vessel pulsation on MRI at present.

Conclusions

We implemented the iMDDSDE-HT2 sequence as a noninvasive and feasible MRI method to assess the CSF MO in healthy participants and in patients with AIS. The proposed method could achieve 3D 1 mm isotropic resolution to identify PVS ROIs and distinguish CSF MO across different pulse phases when gated by a PPU prospectively. We found that CSF MO changes periodically across pulse cycle, and identified pulse phase 3 as being optimal for evaluation of functional changes of GS in further clinical applications.

Funding

The author(s) disclosed receipt of the following financial support for the research, authorship, and/or publication of this article: This work is supported by the National Natural Science Foundation of China (81873749 and 81801072).

Declaration of conflicting interests

The author(s) declared no potential conflicts of interest with respect to the research, authorship, and/or publication of this article.

Authors' contributions

LR: data analysis, study supervision, interpretation of the results, article writing. YH: study supervision, interpretation of the results, article writing. FL: interpretation of the results, article editing. YD: interpretation of the results, article editing. JZ: study design, study supervision, data analysis, interpretation of the results, article writing. XS: interpretation of the results, article editing. WW: study supervision. MW: study design, study supervision, data analysis, interpretation of the results, article writing.

Supplementary material

Supplemental material for this article is available online.

References

1. Lenck S, Radovanovic I, Nicholson P, et al. Idiopathic intracranial hypertension: the veno glymphatic connections. *Neurology* 2018; 91: 515–522.
2. Reeves BC, Karimy JK, Kundishora AJ, et al. Glymphatic system impairment in Alzheimer's disease and idiopathic normal pressure hydrocephalus. *Trends Mol Med* 2020; 26: 285–295.
3. Zou W, Pu T, Feng W, et al. Blocking meningeal lymphatic drainage aggravates Parkinson's disease-like pathology in mice overexpressing mutated α-synuclein. *Transl Neurodegener* 2019; 8: 7.
4. Iliff JJ, Wang MH, Liao YH, et al. A paravascular pathway facilitates CSF flow through the brain parenchyma and the clearance of interstitial solutes, including amyloid beta. *Sci Transl Med* 2012; 4: 147ra111.
5. Mestre H, Tithof J, Du T, et al. Flow of cerebrospinal fluid is driven by arterial pulsations and is reduced in hypertension. *Nat Commun* 2018; 9: 4878.
6. Xie LL, Kang HY, Xu QW, et al. Sleep drives metabolite clearance from the adult brain. *Science* 2013; 342: 373–377.
7. Ringstad G, Valnes LM, Dale AM, et al. Brain-wide glymphatic enhancement and clearance in humans assessed with MRI. *JCI Insight* 2018; 3.
8. Dyke JP, Xu HS, Verma A, et al. MRI characterization of early CNS transport kinetics post intrathecal gadolinium injection: trends of subarachnoid and parenchymal distribution in healthy volunteers. *Clin Imaging* 2020; 68: 1–6.
9. Edeklev CS, Halvorsen M, Løvland G, et al. Intrathecal use of gadobutrol for glymphatic MR imaging: prospective safety study of 100 patients. *AJNR Am J Neuroradiol* 2019; 40: 1257–1264.
10. Kiviniemi V, Wang X, Korhonen V, et al. Ultra-fast magnetic resonance encephalography of physiological brain activity – glymphatic pulsation mechanisms? *J Cereb Blood Flow Metab* 2016; 36: 1033–1045.
11. Zhang W, Zhou Y, Wang J, et al. Glymphatic clearance function in patients with cerebral small vessel disease. *Neuroimage* 2021; 238: 118257.
12. Carotenuto A, Cacciaguerra L, Pagani E, et al. Glymphatic system impairment in multiple sclerosis: relation with brain damage and disability. *Brain* 2022; 145: 2785–2795.
13. Taoka T, Masutani Y, Kawai H, et al. Evaluation of glymphatic system activity with the diffusion MR technique: diffusion tensor image analysis along the perivascular space (DTI-ALPS) in Alzheimer's disease cases. *Jpn J Radiol* 2017; 35: 172–178.
14. Bito Y, Harada K, Ochi H, et al. Low b-value diffusion tensor imaging for measuring pseudorandom flow of cerebrospinal fluid. *Magn Reson Med* 2021; 86: 1369–1382.
15. Lydiane H, Bobby AR, Suzanne LF, et al. The driving force of glymphatics: influence of the cardiac cycle on CSF-mobility in perivascular spaces in humans. *Proc Intl Soc Mag Reson Med* 2020; 28: 0643. https://cds.ismrm.org/protected/20MPresentations/abstracts/0643.html
16. Holz M, Heil SR and Sacco A. Temperature-dependent self-diffusion coefficients of water and six selected molecular liquids for calibration in accurate 1H NMR PFG measurements. *Phys Chem Chem Phys* 2000; 2: 4740–4742.
17. Cao D, Kang N, Pillai JJ, et al. Fast whole brain MR imaging of dynamic susceptibility contrast changes in the cerebrospinal fluid (cDSC MRI). *Magn Reson Med* 2020; 84: 3256–3270.

18. Thomas JH. Fluid dynamics of cerebrospinal fluid flow in perivascular spaces. *J R Soc Interface* 2019; 16: 20190572.
19. Harrison IF, Siow B, Akilo AB, et al. Non-invasive imaging of CSF-mediated brain clearance pathways via assessment of perivascular fluid movement with diffusion tensor MRI. *Elife* 2018; 7.
20. Toh CH and Siow TY. Glymphatic dysfunction in patients with ischemic stroke. *Front Aging Neurosci* 2021; 13: 756249.
21. Zhang J, Zhao H, Xue Y, et al. Impaired glymphatic transport kinetics following induced acute ischemic brain edema in a mouse pMCAO model. *Front Neurol* 2022; 13: 860255.
22. Wen Q, Tong Y, Zhou X, et al. Assessing pulsatile waveforms of paravascular cerebrospinal fluid dynamics within the glymphatic pathways using dynamic diffusion-weighted imaging (dDWI). *Neuroimage* 2022; 260: 119464.